Published in IET Microwaves, Antennas & Propagation
Received on 7th May 2009
Revised on 25th August 2009
doi: 10.1049/iet-map.2009.0283

ISSN 1751-8725

# Aperture blockage and truncation in scanning lens-reflector antennas

*J. Thornton*[1] *S. Gregson*[2] *D. Gray*[3]

[1]*Department of Electronics, University of York, York YO10 5DD, UK*
[2]*Near Field Systems Inc., 20b Albany Road, Fleet, Hampshire GU51 3LY, UK*
[3]*School of Electrical and Computer Engineering, RMIT University, GPO Box 2476, Melbourne Victoria, 3001, Australia*
*E-mail: jt21@ohm.york.ac.uk*

**Abstract:** A lens-reflector antenna comprises a hemispherical dielectric lens with a planar reflector. Beam scanning may be achieved by moving a primary feed around the fixed lens or by rotating the lens reflector with respect to a fixed feed. Truncation of the reflector and obstruction of the aperture by mechanical supports introduce scanning loss. These effects are analysed through a numerical technique where the spherical wave expansion method is used to populate an effective aperture matrix in the near field, which is then modified to account for shadowing effects. The results are verified by a measurement campaign using a scale model and by comparison with the commercial EM solver FEKO.

## 1 Introduction

This investigation is driven by a resurgence of interest in the lens-reflector antenna as a multibeam or scanning antenna for communications applications [1, 2]. This class of antenna uses a planar reflector against the flat surface of a hemispherical dielectric lens, which may be a constant index, stepped-index or Luneburg lens. Ideally, a ground plane of sufficient area recovers the full aperture of a spherical lens whereas in practice a finite ground plane truncates the aperture and thus introduces scanning loss. The geometry is shown in Fig. 1. Also of interest is the case where a mechanical rail surrounds the lens and introduces further aperture blockage, which contributes to scanning loss. Since scanning loss is a critical factor in this class of antenna, we report techniques for both its estimation and mitigation.

Aperture blockage has received attention mostly for reflector antennas. In [3] the effect of blockage by the primary feed is considered by modifying the domain of integration of surface currents so that the masked portion of the aperture is removed; scattering by the supports is then considered by a ray tracing technique. In [4] the scattering by an infinite cylinder in front of a linear array of sub-apertures is considered by expressing the scattered field as a modal expansion: since a linear array is used to model the aperture this approach derives far-field patterns in one axis only for either horizontal or vertical cylinders. Shadowing by zone edges in a Fresnel lens is approached in [5] by computing the total shadowed area rather than diffraction effects at these edges. Aperture efficiency is then expressed from the new effective aperture area: even though the true lens aperture field distribution is not considered, this relatively simple method yields good agreement with measurements. In a similar way, Sachidananda and Ramakrishna [6] treat a blocked region of an aperture as totally absorbing. Another method for blocked reflectors uses the power coupling theorem [7], which combines physical optics (PO) with ray tracing.

In this paper we describe a computationally efficient technique to estimate the effects of ground plane truncation and aperture blocking structures in lens-reflector antennas. We then apply the method to a single-beam scanning antenna for communications to airliners at 45 GHz [1] and then to a multi-beam antenna for satellite communications to trains. The former is motivated by the requirement for a compact 27 dBi scanning antenna without recourse to RF rotary joints or flexible cables and where a constant-index



doi: 10.1049/iet-map.2009.0283

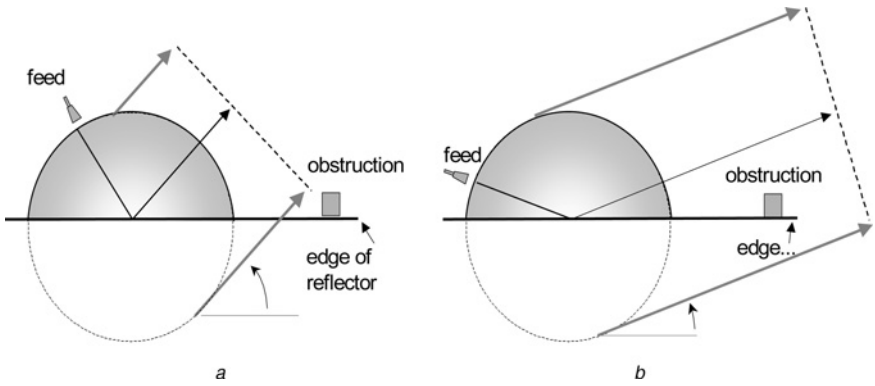


**Figure 1** *Effect of elevation angle on lens-reflector aperture blockage and truncation*

*a* Higher elevation
*b* Lower elevation

lens offers a promising solution. The latter follows the development of a stepped-index lens antenna [2, 8, 9] for satellite communications to trains and where a mechanical rail surrounding the lens introduces partial blockage. The theoretical results are compared with both a measurement campaign and the results using the commercial EM solver FEKO.

## 2 Theoretical approach

For the present work we derive the near-field aperture distribution for a spherical lens and then modify this distribution to account for truncation and blockage. In common with many other approaches, for example [3, 5, 6], the shadowed regions are treated as absorbing.

The spherical wave expansion (SWE) is first used to populate the terms in the near-field aperture, and then the far field is derived using standard transform techniques. These transforms are described in the Appendix. For a given lens and wavelength, the SWE computation is relatively time consuming, whereas the far-field transform is relatively fast and thus, importantly, many different geometries for blocked apertures may be studied quite quickly.

### 2.1 Ground plane truncation

Fig. 2 shows the projection of the finite ground plane onto the aperture plane. Circular and rectangular ground plane geometries are considered (inset in Fig. 2). For a rectangular ground plane the derivation of the truncated region is trivial, and occurs for

$$y' < -r_{gp}\cos(\Psi) \tag{1}$$

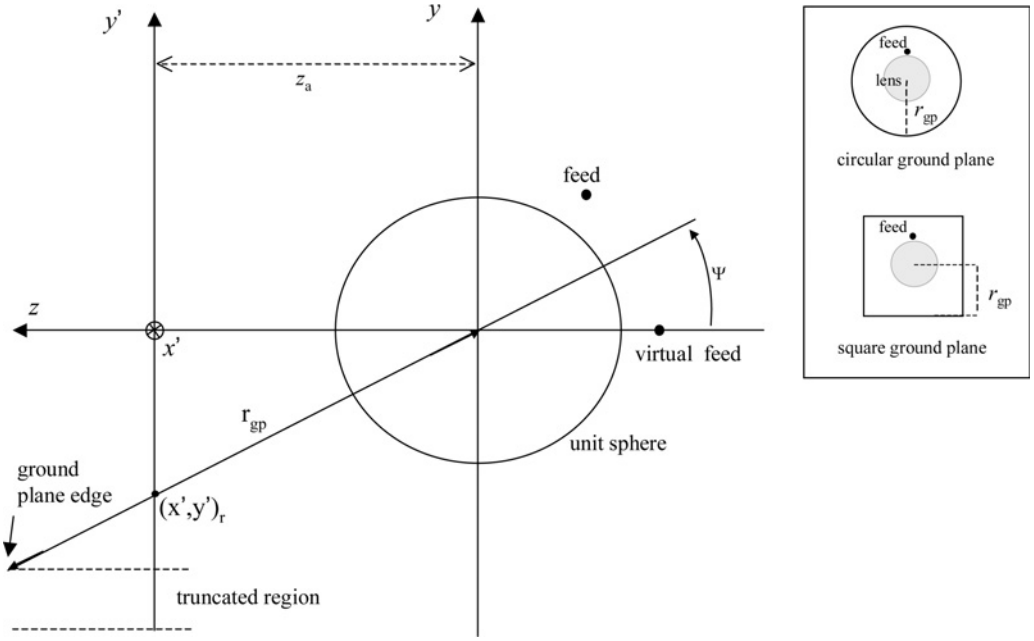


**Figure 2** *Projection of ground plane onto aperture matrix*

where $r_{gp}$ is the distance from the lens centre to the ground plane edge and $\psi$ is the beam scan angle relative to the ground plane.

The finite circular ground plane is less straightforward and requires consideration of the great circle described by the ground plane edge (Fig. 3), which is then projected onto the aperture plane.

Borrowing somewhat from [2] we derive the spherical co-ordinates of this circle using

$$\phi = \arctan(\tan b \sin \Psi) \tag{2}$$

$$\theta = \frac{\pi}{2} - \arcsin(\cos \Psi \sin b) \tag{3}$$

The Cartesian coordinates on a unit sphere are then

$$x_r = \sin\theta \cos\phi \tag{4}$$

$$y_r = \sin\theta \sin\phi \tag{5}$$

Then using the principle of similar triangles, the corresponding Cartesian points in the aperture plane are

$$(x', y')_r = r_{gp}(x, y)_r \tag{6}$$

where $r_{gp}$ is the ground plane radius. It remains to map the ground plane coordinates onto the aperture plane to derive a new field distribution where matrix points in the truncated region are set to zero. This is not yet straightforward because the rail's coordinates $(x', y')_r$ have been expressed as a function of great circle angle $b$, while each point in the aperture matrix is from a Cartesian set in $x'$, $y'$. A simple test for the truncated region can be performed by recourse to an interpolation function for the curve $(x', y')_r$, for example

$$F = \text{Interpolation}[\text{Table}[\{x, y\}, \{b, 0, \pi, 0.01\pi\}]] \tag{7}$$

where the instruction Table[{$x$, $y$}, {$b$, 0, $\pi$, 0.01 $\pi$}] generates a list of Cartesian values {$x$, $y$} as a function of angle $b$ and the interpolation function $F[x]$ then returns values of $y$ associated with a given $x$.

Then, the following test is done for all aperture matrix points $(x', y')$ to zero the truncated points

$$\text{If } |x'| < r_{gp} \text{ and } F[x'] < y' \text{ then } E_{\hat{x}}(x', y') = 0 \tag{8}$$

However, this test is applied only where $y'$ exceeds the points where the ground plane edge lines up with the lens outer edge, that is, where $y' > F[r_{lens}]$ and $r_{lens}$ is the lens radius. These points are labelled $p1$ and $p2$ in Fig. 4*b*. The truncated aperture distributions (3) for rectangular and circular ground planes are shown in Fig. 4, for a 4λ radius constant index lens of dielectric constant 2.5 fed by a two-element end-fire array at $z = -4.3\lambda$. (The lens dimensions are naturally expressed in wavelengths λ.) Here the near-field aperture plane extends over 16λ and lies at $z_a = 4.3\lambda$. (Highest values of $|E_x|$ are shown darkest shade.)

The correct formulation thus far can be tested by comparing the far-field patterns using the direct SWE for the far field and the aperture transform method. These patterns are shown in Fig. 5, which also shows the consequence of a fairly severe aperture truncation because of a low elevation angle of 10°.

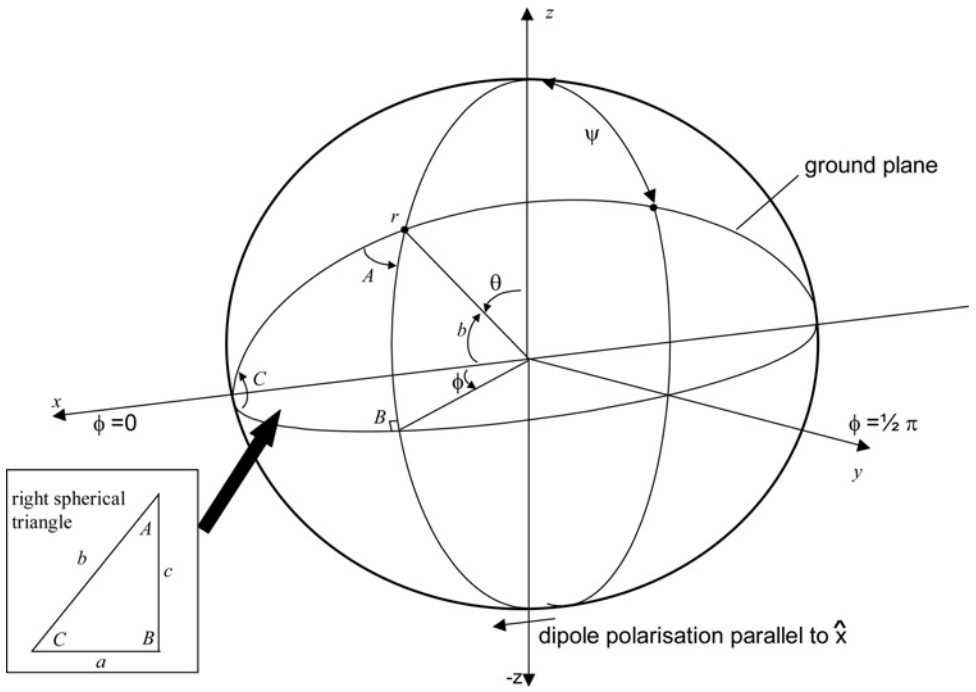


**Figure 3** *Circular ground plane as an inclined great circle, showing spherical coordinates*


*IET Microw. Antennas Propag.*, 2010, Vol. 4, Iss. 7, pp. 828–836

doi: 10.1049/iet-map.2009.0283

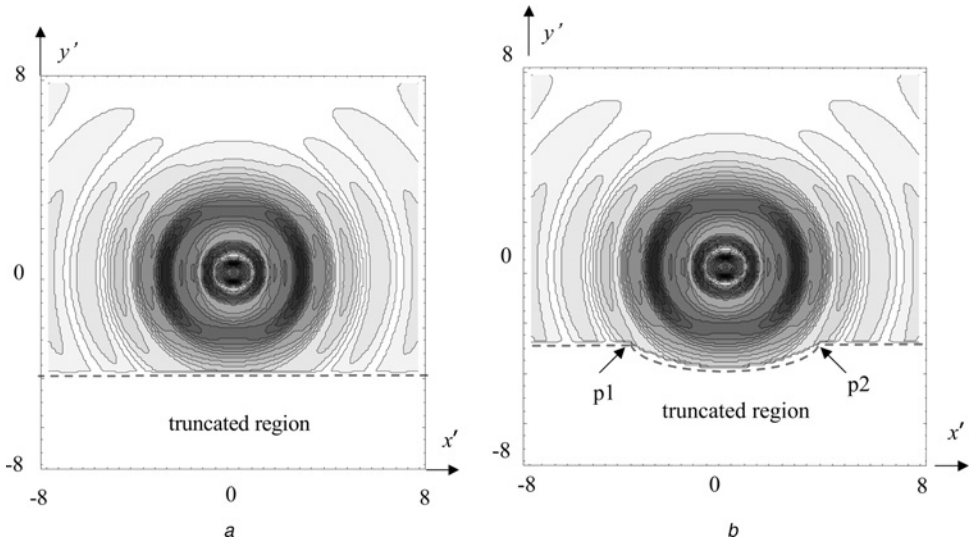


**Figure 4** *Form of aperture distribution for $r_{lens} = 4\lambda$, $r_{gp} = 6\lambda$, $\psi = 45^{\circ}$ for truncated ground planes*

*a* Rectangular
*b* Circular

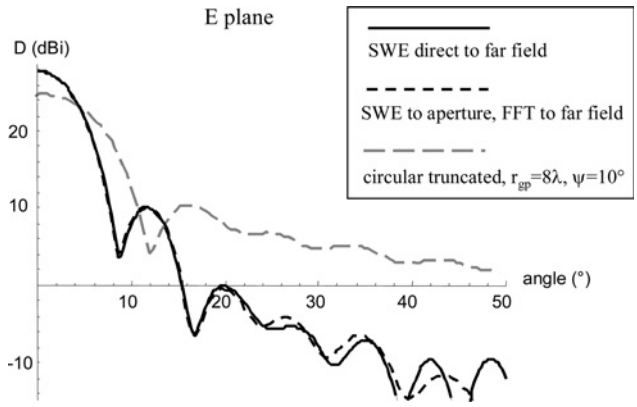


**Figure 5** *Computed radiation patterns, constant-index lens, non-truncated and truncated cases*

As with Fig. 4 the E field is parallel to the ground plane. Arbitrary polarisations can be handled by a simple rotation and thus do not require a new SWE computation for the near-field aperture.

The gain reduction because of the aperture truncation is evident in Fig. 5 and is in effect a scanning loss. Fig. 6 shows sets of results for computed scanning loss against elevation angle for different ground planes. The results from FEKO are also shown.

## 3 Blockage by circumferential rail

Here we are concerned with a dual-beam scanning antenna that has been developed for satellite communications to trains [9, 10], and primarily for geostationary orbit satellites [11]. A mechanical rail surrounds a 61-cm diameter stepped-index lens (Fig. 7) and introduces an unavoidable partial blockage at low elevation angles. The rail provides a support for the motor units that drive the feeds in azimuth, a magnetic strip sensor and for spooled cables that are carried in grooves on the rail's outer edge. (These components were not placed below the ground plane since this would have added to the total height, which is a profound disadvantage on trains.) The extent of the aperture blockage is a function of the rail's height, its distance from the lens edge and the elevation angle. Its height is 36 mm and it sits at a distance 480 mm from the lens centre.

The form of the projection of the azimuth rail onto the aperture plane is similar to that of the circular ground plane (2) to (6), but where the shadowed region now takes the form of a narrow crescent. The rail also has an image because of the ground plane as shown in Fig. 8, where the shadowed region has upper and lower loci respectively $(x', y')_q$ and $(x', y')_p$.

It remains to combine the lens aperture distribution with this shadow region to derive a new aperture distribution. In a similar treatment to that for the circular ground plane, we use interpolating functions to determine the shadowed region. This is shown in Fig. 9, superimposed upon the aperture distribution for the $11\lambda$ radius stepped-index lens of the type in [2]. The aperture plane is here defined by $z_a = 11.5\lambda$, $a = 0.105\lambda$, $A_l = 44\lambda$, leading to a $420 \times 420$ element aperture matrix. This size also ensures that the field strength at the aperture edge has decayed to about $-50$ dB. This geometry was intractable in FEKO because of the electrical size.

Having detailed the computational steps necessary to derive scanning loss for arbitrary rail height, radial distance and elevation angle, it is worth listing some of the

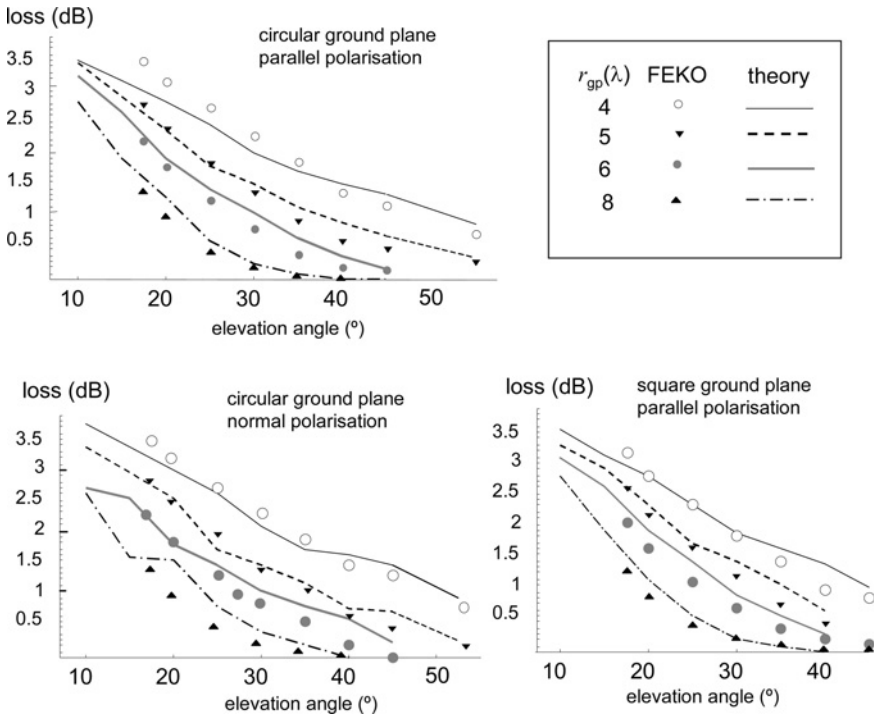


**Figure 6** *Computed scanning loss against elevation angle for different ground planes*

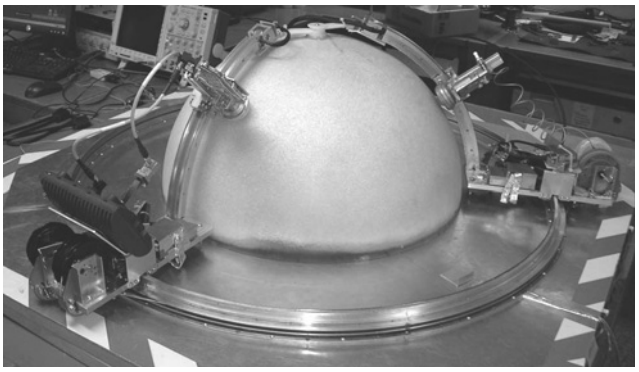

**Figure 7** *Dual beam scanning lens antenna*

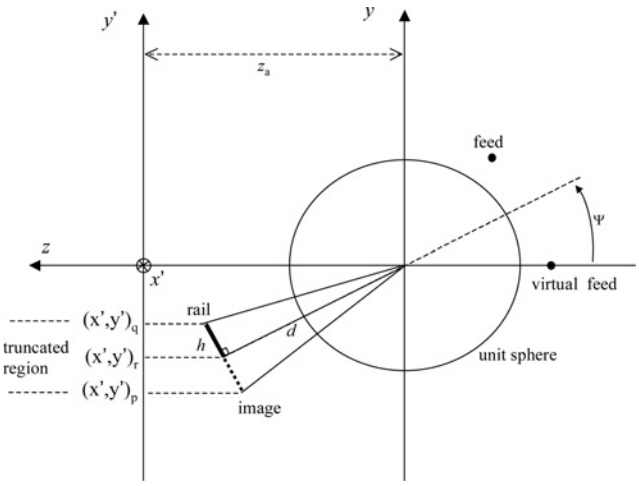


**Figure 8** *Form of projection of azimuth rail onto aperture matrix*

approximations that have necessarily been taken so as to retain a computationally tractable problem:

1. The feed is modelled as a two-element end-fire array of short dipoles in the SWE.

2. We assume that the SWE for a spherical lens is equivalent to that of a hemispherical lens above an infinite plane reflector.

3. We assume that the field incident upon the azimuth rail is either totally backscattered or absorbed, and hence set to zero all shadowed aperture matrix terms.

4. The complexity of the rail's three-dimensional structure is not considered: it is modelled as a flat wall of known height but zero thickness.

We are also concerned with the difference in computed directivity for the unblocked and blocked aperture rather than the absolute accuracy of the computed radiation pattern in either case. Also, the scanning loss is expected to be a small term and will be compared with a series of measurements using a scale model in an anechoic chamber.

## 4 Measurements with scale model

Owing to the size and mass of the 61 cm scanning lens antenna, accurate measurements of directivity with and without the presence of different azimuth rails were not convenient. In contrast, the smaller two-layer lens antenna



doi: 10.1049/iet-map.2009.0283

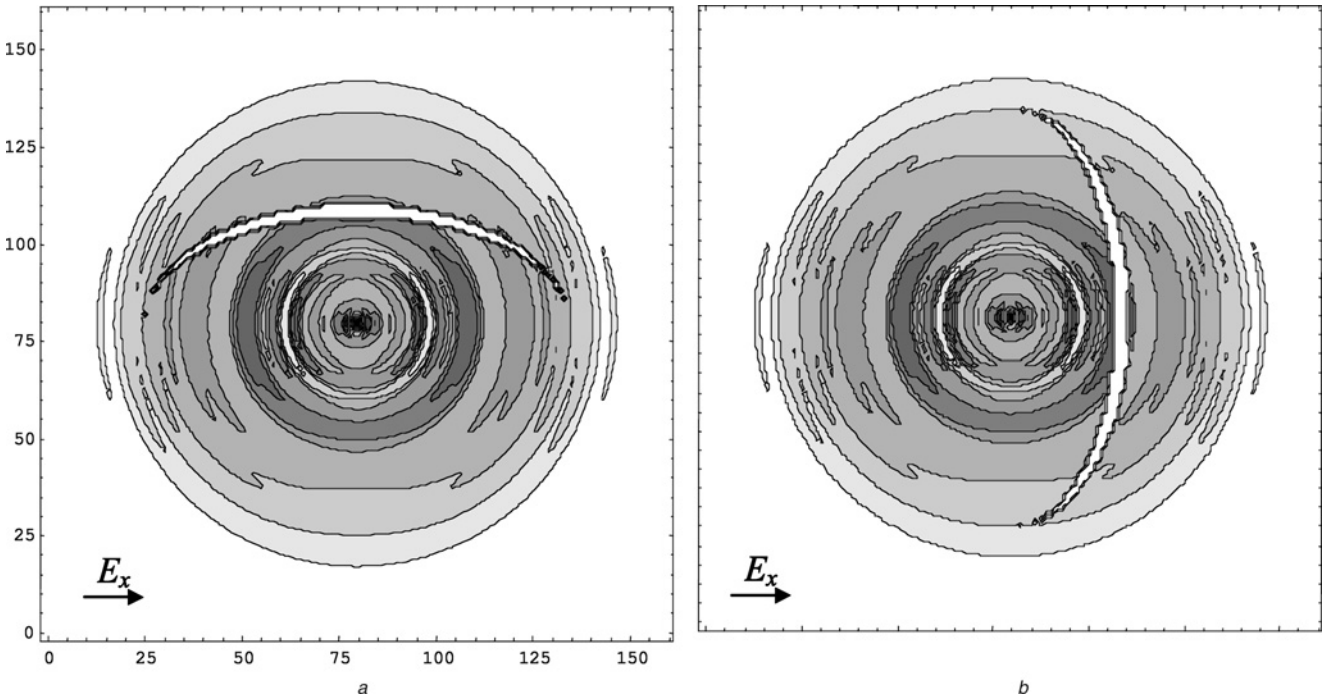


**Figure 9** *Contour plot of aperture matrix $|E_x|$ partially blocked by azimuth rail*
*a* *E*-field parallel to rail
*b* *E*-field perpendicular to rail

of [2] offered a convenient scale model for measurements in an anechoic chamber. The dimensions are shown in Table 1. The frequency scaling term is thus 2.585, scale frequencies of 27–31 GHz equating to operating frequencies of 10.4–12.0 GHz.

One scale model arrangement is shown in Fig. 10, where the model of the significant portion of the azimuth rail is visible as a copper strip. In this experimental arrangement it is also straightforward to alter the dimensions and radial position of the rail so as to also investigate the effect of alternative rail geometries.

The radiation patterns for the antenna shown in Fig. 10, with and without the azimuth rail, are shown in Fig. 11. Here the source polarisation is vertical, that is, perpendicular to the ground plane and rail model. These patterns are fairly typical of what has been observed over many measurements: a slight decrease in peak directivity and small growth in sidelobe levels. The measured

**Table 1** Antenna dimensions (mm)

| | Full size | Scale model |
|---|---|---|
| lens diameter | 610 | 236 |
| rail height | 36 | 14 |
| rail radius | 480 | 186 |

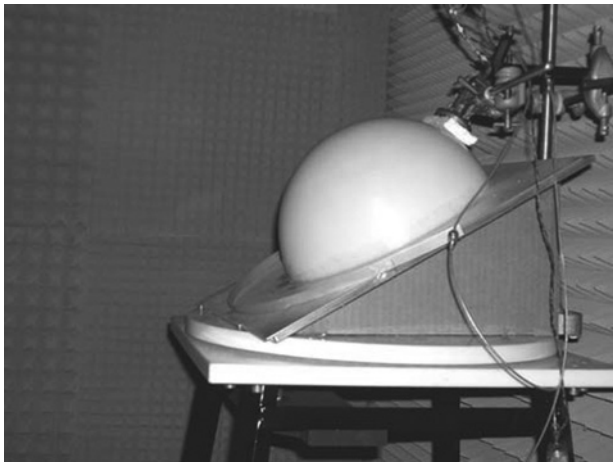

**Figure 10** *Scale model of lens antenna with azimuth rail, 30° elevation*

scanning loss was, respectively, 0.3 and 0.4 dB for vertical ($E_v$) and horizontal ($E_h$) polarisation, which corroborates the computed values.

The scanning loss results shown in Fig. 12 follow the expected trend that the loss tends to increase with decreasing elevation angle.

Further measurements were carried out to investigate the alternative azimuth rail geometries so as to quantify the reduction in scanning loss that could be expected.

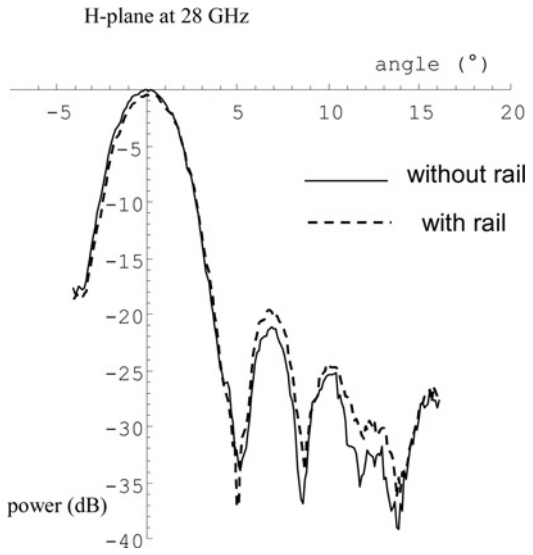


**Figure 11** *Typical radiation patterns for scale model at 28 GHz, 14 mm rail*

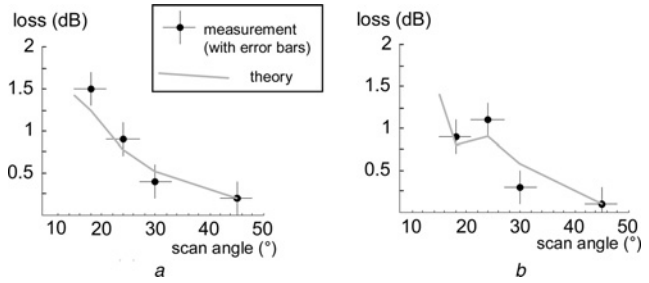


**Figure 12** *Scanning loss due to 14 mm rail at 28 GHz*

*a* Parallel polarisation
*b* Perpendicular polarisation

Rail models of height 10 and 5 mm were investigated for various radial distances so as to assess the trade-off between scanning loss and space occupied by hardware. The theoretical and measured scanning loss for two polarisations and two elevation angles are shown in Table 2 for a frequency of 28 GHz. A smaller set of data for a few measurements taken at 31 GHz is also shown in Table 3.

**Table 3** Scanning loss for rail distance 68 mm, 24° elevation and at 31 GHz

| Rail height, mm | Loss $E_h$ (dB) | | Loss $E_v$ (dB) | |
|---|---|---|---|---|
| | Theory | Measurement | Theory | Measurement |
| 14 | 0.79 | 0.9 | 0.96 | 1.2 |
| 10 | 0.58 | 0.7 | 0.62 | 0.6 |

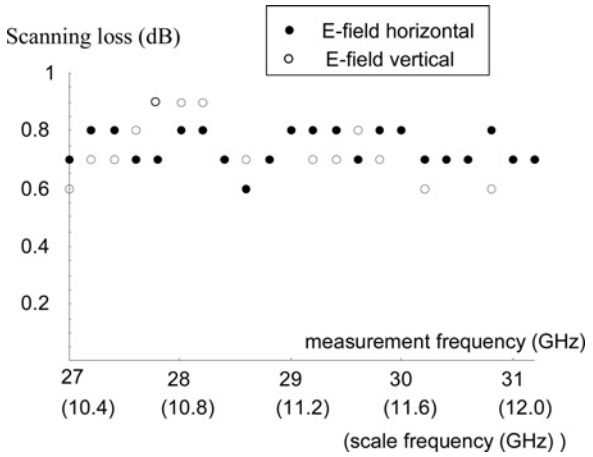


**Figure 13** *Measured scanning loss against frequency for 10 mm rail at radius 186 mm and 24° elevation*

Finally, some measurement data for scanning loss against frequency are presented in Fig. 13 for a single rail geometry. The model rail height of 10 mm would correspond to a full size height of 26 mm. In this investigation we were looking for any strong frequency dependence, none of which were found over this frequency range.

**Table 2** Scanning loss, theory and measurement, for alternative rail geometries at 28 GHz

| Rail distance from lens edge, mm | | 24° elevation, loss, dB | | | | 18° elevation, loss, dB | | | |
|---|---|---|---|---|---|---|---|---|---|
| | | $E_h$ | | $E_v$ | | $E_h$ | | $E_v$ | |
| | | Theory | Measurement | Theory | Measurement | Theory | Measurement | Theory | Measurement |
| 10 mm rail height | 10 | 1.12 | 1.3 | 1.19 | 1.4 | 1.37 | 1.5 | 0.95 | 1.2 |
| | 68 | 0.59 | 0.7 | 0.72 | 0.9 | 0.98 | 1.3 | 0.79 | 0.9 |
| | 118 | 0.38 | 0.3 | 0.43 | 0.5 | 0.71 | 0.9 | 0.71 | 0.8 |
| 5 mm rail height | 10 | 0.41 | 0.4 | 0.42 | 0.6 | 0.41 | 0.3 | 0.59 | 0.8 |
| | 68 | 0.25 | 0.2 | 0.24 | 0.4 | 0.29 | 0.2 | 0.51 | 0.7 |
| | 118 | 0.13 | 0.0 | 0.22 | 0.2 | 0.19 | 0.2 | 0.38 | 0.5 |


*IET Microw. Antennas Propag.*, 2010, Vol. 4, Iss. 7, pp. 828–836
doi: 10.1049/iet-map.2009.0283

# 5 Conclusions

Lens-reflector antennas can offer an attractive solution for scanning antennas at microwave or millimetre wave frequencies. A single feed lens can scan a beam without recourse to rotary RF joints, whereas a multi-feed variant offers multiple beams by sharing the lens aperture. In either case, the finite reflector (ground plane) gives rise to scanning loss at low elevation angle because the aperture becomes truncated. This loss has been estimated using a numerical method where a near-field planar aperture distribution is first derived using SWE, and later modified by removing terms in the truncated region. The far field is then derived using a standard transform. Results for both circular and square ground planes and an eight wavelength diameter hemispherical lens have been presented. Polarisation of an incident field either parallel or perpendicular to the ground plane was considered. The commercial solver FEKO was used to corroborate the theoretical method and the agreement was good. Ground plane extensions between zero, one-quarter, one-half and one times the lens radius were examined, and the scanning loss varied between zero and almost 4 dB depending on scan angle, the lowest angle studied being 10°.

The method was then adapted to consider the shadowed region of the aperture introduced by a mechanical rail, which surrounds a 61-cm diameter lens in a dual-beam scanning antenna. At 10.8 GHz and upwards this problem is intractable in FEKO because of electrical size, but theoretical results were compared with a suite of measurements on a scale model at around 28 GHz. This also allowed a comparison of different rail geometries and thus indicates how scanning loss can be reduced by simplifying and making the rail smaller. In the example presented, the rail height is 36 mm and the scanning loss it introduces starts to become significant at a 30° elevation angle, where both theory and scale model measurement indicate a loss of 0.4 dB, increasing to 1.5 dB measured at 18° elevation. Should the azimuth rail be reduced to a height of 13 mm, the scanning loss at 18° elevation angle should not exceed about 0.7 dB, although this again varies slightly with polarisation and frequency. This loss can be further reduced by increasing the distance between the lens and the rail.

Scanning loss is often a critical performance metric for antennas of the type discussed, and the techniques and results presented should be of general applicability for assessing various lens and ground plane geometries.

# 6 Acknowledgment

Thanks to Andy White and staff of Technical Support Services, Department of Electronics, University of York, Brent Wilkinson of the Department of Physics mechanical workshop, Graham Long, and Maarten Van Der Vorst the ESA programme manager for the Innovation Triangle Initiative. This work was supported in part by the European Space Agency under Contract No. 20836/07/NL/CB. FEKO simulations were undertaken by D. Gray at NICT, Japan.

# 7 References

[1] GRAY D., THORNTON J., TSUJI H.: 'Mechanically steered lens antennas for 45 GHz high datarate airliner-ground link'. EHF-AEROCOMM/GLOBECOM 2008, New Orleans, USA, 30 November–4 December 2008

[2] THORNTON J.: 'Wide-scanning multi-layer hemisphere lens antenna for Ka band', *IEE Proc. Microw., Antennas Propag.*, 2006, **153**, (6), pp. 573–578

[3] KO W.L., MITTRA R., LEE S.W.: 'Aperture blockage in reflector antennas', *IEEE Trans. Antennas Propag.*, 1984, **AP-32**, (3), pp. 282–287

[4] WINCHELL S.G., DAVISON D.: 'Near-field blockage of an ultralow sidelobe antenna', *IEEE Trans. Antennas Propag.*, 1980, **AP-28**, (4), pp. 451–459

[5] PETOSA A., ITTIPIBOON A.: 'Shadow blockage effects on the aperture efficiency of dielectric Fresnel lenses', *IEE Proc.-Microw. Antennas Propag.*, 2000, **147**, (6), pp. 451–454

[6] SACHIDANANDA M., RAMAKRISHNA S.: 'Constrained optimization of monopulse circular aperture distribution in the presence of blockage', *IEEE Trans. Antennas Propag.*, 1983, **AP-31**, (2), pp. 286–293

[7] MIGLIOZZI M., PARINI C.G., RAYNER M.R.R.: 'A new efficient method for the analysis of the far field of a satellite earth station antenna in the presence of near field obstacles'. IEE Int. Conf. on Antennas and Propagation (ICAP), April 2001 pp. 361–364

[8] THORNTON J.: 'Scanning Ka-band vehicular lens antennas for satellite and high altitude platform communications'. 11th European Wireless Conf., 10–13 April 2005

[9] THORNTON J.: 'Tracking multi-beam lens antenna: the gain of a dish in half the height'. IET Broadband on Trains Seminar, IET, Savoy Place, London, 23 April 2009

[10] THORNTON J., WHITE A.D., GRAY D.: 'Multi-beam lens-reflector for satellite communications: construction issues and ground plane effects'. European Conf. on Antennas and Propagation (EUCAP09), 23March 2009, pp. 1377–1380

[11] THORNTON J., WHITE A.D., TOZER T.C.: 'Development of dual beam tracking lens antenna for satellite communications to trains'. 27th Int. Communications Satellite Systems Conf. (ICSSC 2009), 1–4June 2009

[12] BALANIS C.A.: 'Antenna theory, analysis and design' (Wiley, 2005, 3rd edn.), pp. 1014–1021

[13] GREGSON S., MCCORMICK J., PARINI C.: 'Principles of planar near-field antenna measurements', *IET, Electromag. Waves Ser.*, 2008, **53**, p. 120

[14] GREGSON S., MCCORMICK J., PARINI C.: 'Principles of planar near-field antenna measurements', *IET, Electromag. Waves Ser.*, 2008, **53**, pp. 138–141, p. 358

[15] MEIJERING E.H.W., NIESSEN W.J., VIERGEVER M.A.: 'The sinc-approximating kernels of classical polynomial interpolation'. Proc. Int. Conf. on Image Processing (ICIP), October1999, vol. 3, pp. 652–656

## 8 Appendix: Notes on aperture transforms

Although spectral techniques may under certain circumstances be used over other smooth surfaces, they are most commonly associated with sampling over planar surfaces, as used here. For a given spherical lens, the SWE method is used to populate terms for electric field for all points across the aperture matrix of length $A_l$.

This plane has axes $x'$, $y'$ parallel to the $x$, $y$ plane and centred at $x' = 0$, $y' = 0$, $z' = z_a$ (Fig. 14).

Since the SWE method is naturally expressed in spherical coordinates, the usual transformation from spherical to Cartesian coordinates is encountered on deriving the electric field in the aperture plane:

$$E_{\hat{x}}(x', y') = E_{\hat{\theta}} \cos\theta \cos\phi - E_{\hat{\phi}} \sin\phi + E_{\hat{r}} \sin\theta \cos\phi$$

Having populated the terms of the aperture matrix for co-polarised electric field $E_{\hat{x}}$ these may be manipulated to emulate the effect of objects that partially obstruct or truncate that aperture. The shadowed regions are treated as absorbing. The far field is then derived by the usual near-field to far-field transform for a planar aperture [12].

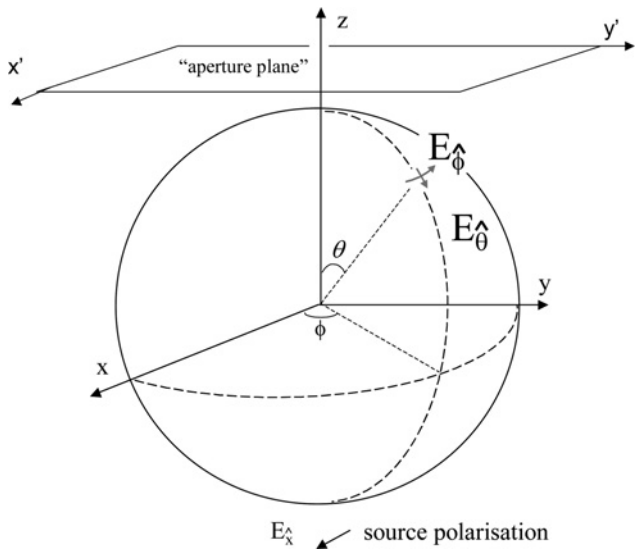


**Figure 14** *Lens and aperture coordinate system*

The method is analogous to conducting a near-field planar scan of the antenna, either with or without the presence of the obstructions, and then computing the far field from the measured near field. The form of the planar aperture is derived from a few well-established rules:

1. The extent of the near-field sampling area can be determined from the maximum angular angle: $\theta_{max} = \arctan(A_l/2\Delta z)$ where $\Delta z$ is the separation between the antenna and the sampling plane.

2. As reactive fields are attenuated with distance (56.4 dB/wavelength or more), the separation between the radiator and the sampling plane will limit the resolution of the sampled fields and the highest order plane wave component. However, at present we are only interested in fields that propagate to the far-field and so this separation can be as large as 3 wavelengths.

3. Although the maximum value of sample spacing is determined by the highest propagating plane wave component and results in a sample spacing of half wavelength in each axis [13], we need here a finer spacing so as to capture the geometry of the electrically small blocking structure.

Computation of the SWE for $E_x$ across the aperture plane is relatively time consuming depending on lens and aperture size. From considerations of symmetry, it is necessary only to compute one quadrant of the aperture. However, this need be performed only once for a given lens geometry and frequency. The transform to the far field (3) is relatively fast and so, importantly, many variants of the geometry of the ground plane or blocking objects can be analysed quite quickly. In computing the far field we retained the discrete Fourier transform (DFT) rather than the rearranged form, which is the fast Fourier transform (FFT) since the speed of the latter is bought at the price of the data being sampled on a plaid, equally spaced grid. The output of the FFT is sampled on a regular direction cosine grid, which is not convenient for antenna patterns when an angular sampling space is usually required, so the pattern data must be interpolated from the direction cosine grid onto the desired angular grid. If this is implemented using approximation (i.e. piecewise polynomial interpolation) inaccuracies can be introduced into the results; alternatively, if sampling theory interpolation is used, this can be as intensive as the direct DFT. Thus, for these reasons, when using powerful modern computers, the computational effort required by the DFT can be an acceptable price to pay, particularly when recurrence relations are used to improve the efficiency of the algorithm [14, 15].



doi: 10.1049/iet-map.2009.0283